Progress In Electromagnetics Research, Vol. 111, 447–465, 2011

EXPERIMENTAL BREAST TUMOR DETECTION USING NN-BASED UWB IMAGING

S. A. Alshehri

Department of Computer and Communication Systems Engineering
Faculty of Engineering, Universiti Putra Malaysia
Serdang, Selangor 43400, Malaysia

S. Khatun

Department of Computer Systems & Networks
Faculty of Computer Systems & Software Engineering
Universiti Malaysia Pahang
Gambang, Kuantan, Pahang 26300, Malaysia

A. B. Jantan

Department of Computer and Communication Systems Engineering
Faculty of Engineering, Universiti Putra Malaysia
Serdang, Selangor 43400, Malaysia

R. S. A. Raja Abdullah

Wireless & Photonic Networks Research Centre
Universiti Putra Malaysia, Serdang, Selangor 43400, Malaysia

R. Mahmood

Department of Imaging, Faculty of Medicine and Health Sciences
Universiti Putra Malaysia, Serdang, Selangor 43400, Malaysia

Z. Awang

Microwave Technology Center, Faculty of Electrical Engineering
Universiti Teknologi Mara, Shah Alam, Selangor 40400, Malaysia

Received 1 November 2010, Accepted 16 December 2010, Scheduled 22 December 2010
Corresponding author: Sabira Khatun (sabira@ump.edu.my).

Abstract—This paper presents a system with experimental complement to a simulation work for early breast tumor detection. The experiments are conducted using commercial Ultrawide-Band (UWB) transceivers, Neural Network (NN) based Pattern Recognition (PR) software for imaging and proposed breast phantoms for homogenous and heterogeneous tissues. The proposed breast phantoms (homogeneous and heterogeneous) and tumor are constructed using available low cost materials and their mixtures with minimal effort. A specific glass is used as skin. All the materials and their mixtures are considered according to the ratio of the dielectric properties of the breast tissues. Experiments to detect tumor are performed in regular noisy room environment. The UWB signals are transmitted from one side of the breast phantom (for both cases) and received from opposite side diagonally repeatedly. Using discrete cosine transform (DCT) of these received signals, a Neural Network (NN) module is developed, trained and tested. The tumor existence, size and location detection rates for both cases are highly satisfactory, which are approximately: (i) 100%, 95.8% and 94.3% for homogeneous and (ii) 100%, 93.4% and 93.1% for heterogeneous cases respectively. This gives assurance of early detection and the practical usefulness of the developed system in near future.

1. INTRODUCTION

Breast cancer detection using Ultrawide-Band (UWB) imaging is under investigation [1–12]. The main principle in UWB imaging application is the use of contrast in dielectric properties among different breast tissues [5, 6, 13]. Several successful works have been done using numerical breast model [2, 3, 6]. Byrne et al. conducted an investigation on several of these numerical models and the Confocal Microwave Imaging (CMI) algorithms to evaluate the performance of each beamformer [14]. O'Halloran et al. suggested an improvement to some of these algorithms by selecting subset of the received scattered signals to overcome the heterogeneous tissues effects [15]. This method faces difficulty to distinguishing between tumor and glandular tissue effect. Klemm et al. and Lazaro et al. stated that up to date there have been few experimental breast-imaging radar systems reported in the open literature [16, 17]. To the best of our knowledge, there has been only one attempt to use heterogeneous breast phantom in UWB imaging system [18] with several limitations. First, the authors stated that the whole heterogeneous materials were not suitable to mimic the breast phantom. Second, the considered shape of the phantom was cylindrical and not a realistic breast shape. In addition,

in order to make correct detection, they had to get the phantom image twice (with and without tumor) which would not be feasible for clinical implementation. Experimental works have been reported in [1, 4, 5, 7, 18] for homogeneous breast phantom using some devices including costly Vector Network Analyzer (VNA). However, the widely used confocal method depends on the knowledge of the exact size and relative permittivity of the homogeneous breast under test to determine the UWB signals travelling time. This is necessary for any signal focusing algorithm. The relative permittivity is obtainable in the experimental work but difficult to be known clinically. Also the actual human breast is heterogeneous (glandular) and not homogeneous. This makes it very hard to be implemented clinically. So far, mixture of various percentages of soy oil and gelatin are the mostly used materials to mimic breast fatty tissues. A different percentage of oil and water have been used to construct heterogeneous and tumor tissues in some works [1, 5, 7, 18, 19]. In almost all the previous studies, the breast phantoms have been constructed to be used for relatively longer time. But it is found that the water content migrates with time which may produce inconsistent results [7, 18] to use those phantoms for longer duration.

Here, we propose a user friendly and cost effective UWB imaging system for early breast tumor detection without using VNA. It consists of commercial UWB signal generator with transceiver, a developed complete software module including Neural Network (NN) model for detection and two breast phantoms for temporary and immediate use. We have fabricated homogenous and heterogeneous breast phantoms for our experiment with available low-cost materials, and minimum effort.

The paper is organized as follows. The next section presents the full system including the method of constructing the breast phantoms and tumor tissues, experimental data collection, NN training and testing, followed by results, and finally the conclusion.

2. SYSTEM SCENARIO

2.1. The Experimental System Configuration

Figure 1 shows the experimental system set-up. The UWB transmitter (Tx) and receiver (Rx) are connected to a PC using Ethernet hub and can be controlled through the PC. The breast phantom is placed between the transmitter and receiver. The tumor is placed along the line between the transmit and receive antennas initially. The software interface with the UWB devices gives the ability to run both transmitter and receiver Graphical User Interface (GUI)

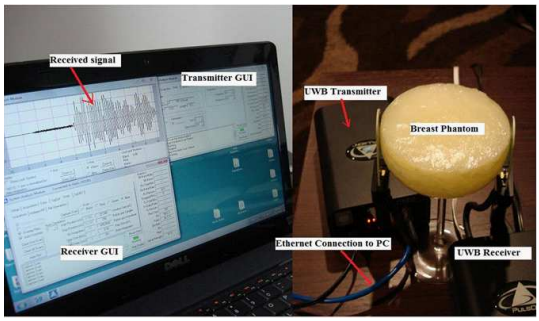

Figure 1. Experimental system set-up scenario.

simultaneously. At any time, the received signal waveform can be captured and seen in the PC monitor through GUI (as shown in Figure 1) without the use of VNA.

2.2. UWB Transceiver

We have used Time Domain product called UWB PulsOn device [20] as UWB transmitter and receiver. It works with center frequency of 4.7 GHz and bandwidth of 3.2 GHz. It uses Omni directional antennas, packet format for transmission and shows the received waveform in time domain. Usually, the Omni directional antennas shows lower efficiency, hence we have designed and used UWB directional antennas for performance optimization (this is not the focus of this paper and not discussed here).

2.3. Material Investigation for Breast Phantom and Tumor Construction

In [8], the dielectric properties (permittivity and conductivity) of the breast tissues were obtained from [21]. The exact dielectric properties values are not important. The most important metrics are the ratios between the dielectric properties values for different breast tissues [4, 5], which is approximately, fatty-tissue : skin : glandular-tissue : tumor $\sim$ 1 : (1.5 to 5) : (2 to 4) : (9 to 10 or more) [7, 22]. According to some research, even these ratios are not fixed and may vary [2, 5, 6, 13, 18, 22, 23].

The dielectric properties are dependent on the water contents of the tissue [18, 22, 24, 25]. We have tried to create tumor and glandular tissues with different dielectric constant values by changing the water to wheat flour ratio. By mixing water and wheat flour in various weight

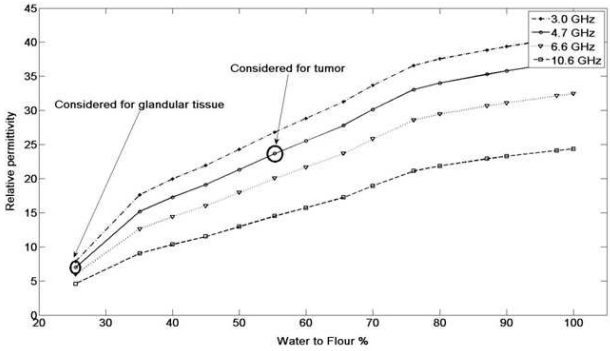

Figure 2. Relative permittivity for various water to wheat flour ratios.

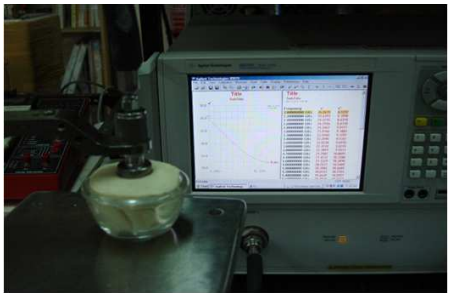

Figure 3. Agilent N5230A VNA with HP 85070B dielectric probe.

quantities, we can get mixtures with various dielectric properties. Figure 2 shows the water to wheat flour ratios versus the permittivity at certain frequencies. The measurement is done using Agilent N5230A VNA and HP 85070B dielectric coaxial probe as show in Figure 3. In terms of permittivity ratio, we have found that petroleum jelly and a specific type of glass are closer to the breast fatty tissue and the skin respectively. The glass is lossless material and its dielectric property is considered according to [26]. It is only 1.6 (mm) thick, so its lossless effect is minimal. Figures 4 and 5 show the permittivity and conductivity of various materials in the frequency range of 2–12 GHz. The dielectric properties of the considered materials at 4.7 GHz frequency are shown in Table 1.

2.3.1. Tumor Tissue Construction

There are two tumor types namely: benign and malignant. They have different features. Conceicao et al. tried to distinguish between them based on radar target signatures [27]. In our study, we have only used

Table 1. Dielectric properties of the used materials at 4.7 GHz.

Breast phantom part	Material	Permittivity	Conductivity (S/M)
Fatty tissue	Pure petroleum jelly	2.36	0.012
Tumor	Mixture of water and wheat flour (55%)	23	2.57
Skin	Glass	3.5–10	negligible

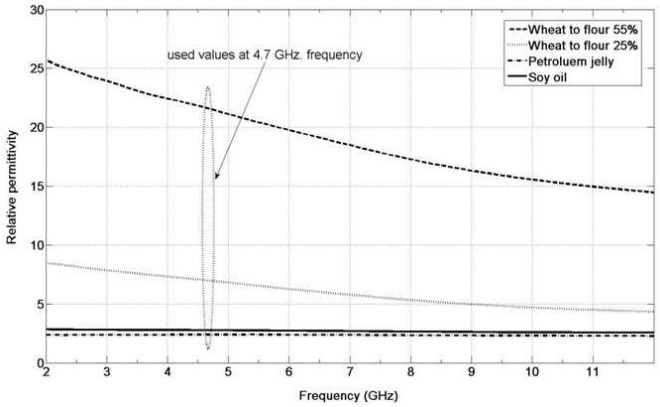

Figure 4. Relative permittivity of the various used materials.

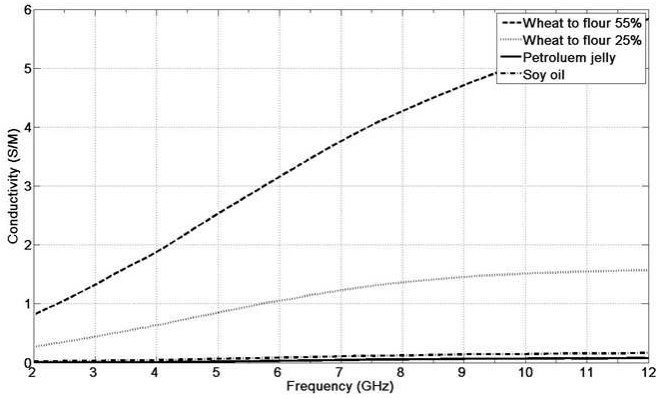

Figure 5. Conductivity of the various used materials.

malignant tissue and did not consider the difference between these two types.

Tumor is constructed by mixing 10 g of wheat flour to 5.5 g of water. This produces a mixture of water to wheat flour ration 55% with permittivity 23 and conductivity of 2.57 (S/M) at frequency 4.7 GHz. This mixture is used to construct tumor for various sizes and inserted in breast phantoms for experimental detection. From Figure 2 and Table 1, the permittivity of this mixture is 23. So, the tumor to fatty breast tissue permittivity ratio is 9.7 : 1 which is close to the value reported in [7]. Table 2 shows the considered tumor sizes corresponding to their locations inside breast phantoms. Only x-coordinate of tumor is varied to ease our experiment.

Table 2. Combinations of tumor size and location used for experiments. The surface of the glass is assumed to be $z = 0$ (mm).

Tumor sizes in diameter (mm)	Tumor locations (x, y, z) (mm) (w.r.t transmitter)			
1.0	$(10, 0, -4)$	$(20, 0, -4)$	$(50, 0, -4)$	$(70, 0, -4)$
2.0	$(15, 0, -4)$	$(20, 0, -4)$	$(55, 0, -4)$	$(75, 0, -4)$
4.5	$(10, 0, -4)$	$(20, 0, -4)$	$(60, 0, -4)$	$(75, 0, -4)$
6.0	$(25, 0, -4)$	$(40, 0, -4)$	$(65, 0, -4)$	$(75, 0, -4)$
7.5	$(30, 0, -4)$	$(40, 0, -4)$	$(60, 0, -4)$	$(70, 0, -4)$

2.3.2. Homogenous Breast Phantom

A glass of hemispherical shape with 100 (mm) diameter, 50 (mm) height and about 1.6 (mm) thick is used as skin. Its shape is similar to patient breast in prone position. Here, the prone position is considered due to its better performance in terms of Single-to-Clutter Ration (SCR) and Signal-to-Mean Ration (SMR) [28].

To imitate the fatty breast tissue, it is filled with pure petroleum jelly. Figure 6 shows a 4.5 (mm) tumor located at 75 (mm) from transmitter. Two other tumors with size 4.5 (mm) and 1 (mm) can be seen at the upper and lower right corners of the same figure respectively.

2.3.3. Heterogeneous Breast Phantom

The breast usually contains glandular tissues which have higher dielectric properties values [22] than the adipose tissues. It has been decided to use 100 : 50 : 37 a mixture of petroleum jelly, soy oil

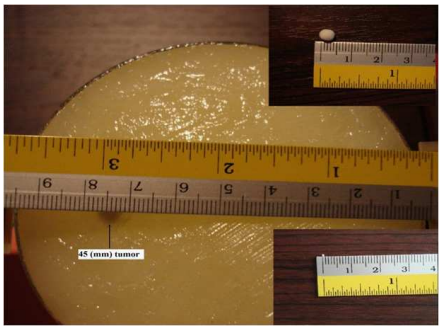

Figure 6. A 4.5 (mm) tumor located at 75 (mm) from transmitter. A 4.5 (mm) and 1 (mm) tumors are shown in upper and lower right corners respectively.

Figure 7. Heterogeneous construction materials before mixing.

Table 3. Heterogeneous breast fatty tissue mixed materials at 4.7 GHz.

Breast fatty tissue contents	Weight (g)	Permittivity	Conductivity (S/M)
Petroleum jelly	152.3	2.36	0.012
soy oil	76.1	2.7	0.061
Water to flour ratio (25%)	57	6.98	0.785

and water to wheat flour ratio of 25% to make the breast totally heterogeneous. Figure 7 shows the used materials before mixing and Table 3 shows the materials with their weights used to mimic this part. The rest of the experiment is similar to the setup used for homogenous case.

We have not included the chest representation on our phantom because of the difficulty to insert the tumor inside the phantom. Here, the effect of the chest is minimal since in our measurement, the tumor is detected only when it is along the straight line between the transmitter and receiver.

2.4. Discrete Cosine Transform and Feature Extraction

In [8], UWB signals in time domain were used. Those signals were sampled to obtain the feature vector to train the NN model. PulsOn device does not show the time relation between the transmitted and the received signals, it only shows the waveform. So, it is impossible to sample the received signals at the same instance of time. The

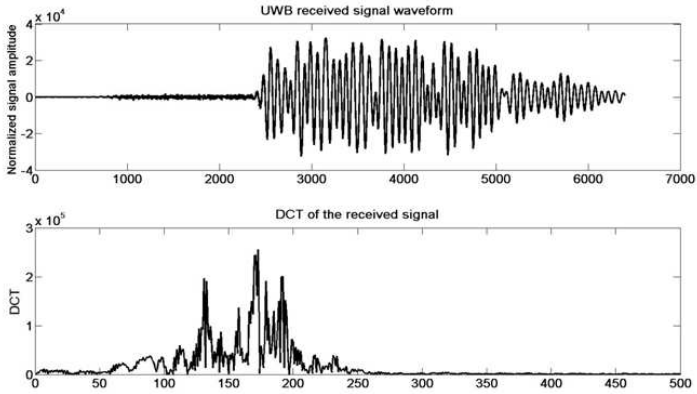

Figure 8. UWB signal waveform received by UWB device and its DCT for tumor of size 1 (mm) placed at a distance 50 (mm) from transmitter.

Discrete Cosine Transform (DCT) is a sum of infinitely many cosines basis functions in different frequencies with varying amplitudes [29]. It can approximate any signal, hence we have used DCT. Applying DCT to the same data obtained through simulation in [8], gives tumor existence, size and location detection rate at about 100%, 86.9% and 80.4% respectively. Figure 8 shows a received UWB signal correspond to tumor with size 1 (mm) located at 50 (mm) from transmitter and its DCT.

2.5. Neural Network

Initially, a two-layer simple back-propagation feed-forward NN model has been constructed and trained for experimental tumor existence with size and location detection individually. It had one hidden layer of 3 nodes and an output layer with one node for detecting tumor location or size respectively. Then, these two NN modules were integrated and tested to make one with higher efficiency. The developed model and considered parameters are similar to [8] except the number of layers. Existence of tumor is decided by the positive output from both NN architectures. MatLab 7 is used to calculate DCT and to construct the NN model. Each received UWB signal using the UWB transceiver consists of 6400 points. Since large DCT values appear in the range of 50-300, it has been used to construct the feature vector of the NN. The generalization test of the NN model has been performed using cross-validation method.

2.6. The Experimental Data Collection and Detection

The procedures to collect the data and to detect the tumor in 2D are similar to the procedures presented in [8]. However, in this work, the feature vector contains the DCT of the signals. The whole system for experimental data collection and detection process is shown in Figure 9. Here, only the commercial UWB Tx-Rx with PC connectors is utilized, the rest are proposed and developed by us eliminating the need of

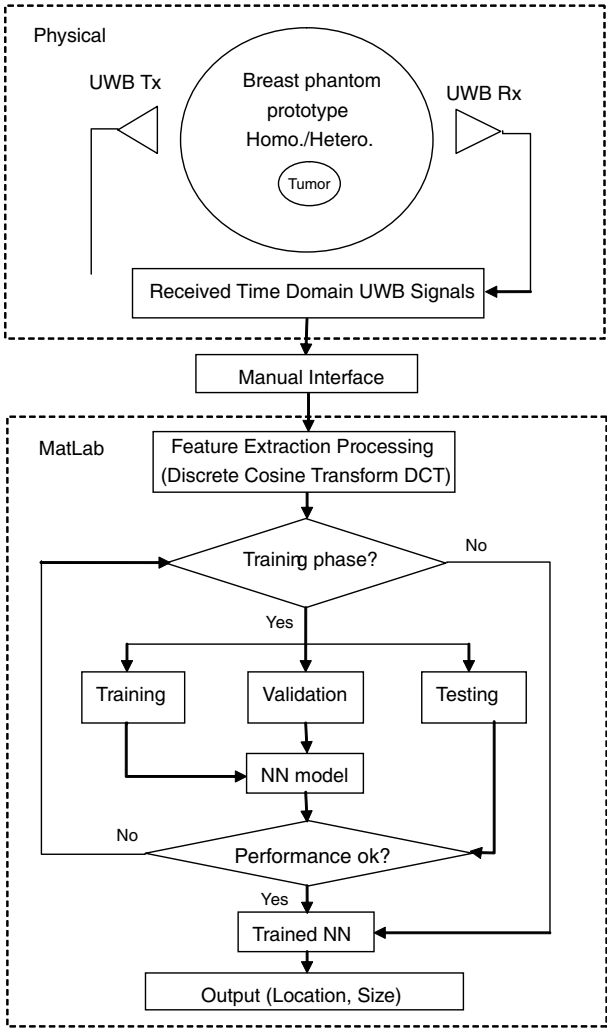

Figure 9. Experimental and data collection process.

VNA. The system prototype consists of a UWB Tx-Rx, one PC and our developed software package module (installed in the PC). Hence the system is VNA free, user friendly and affordable in terms of cost.

To generate experimental data, the following steps are used:

1) The UWB transmitter and receiver are placed diagonally at opposite sides of the breast phantom (Figure 9).

2) Activate the transmitter through PC to transmit 4.7GHz (center frequency) UWB signal.

3) Capture the received signal from the receiver through PC and save it.

4) Send the received signals to processing module for DCT and best complement detection (when the tumor is in line with Tx-Rx pair [8]).

5) Send the processed data to NN model for training, validation and testing until the performance is satisfactory.

6) Repeat the Steps 1–6 for each pair of tumor size and location in Table 2. The UWB transceiver is used to transmit and receive three different UWB signals to generate as maximum number of signals as possible for better NN training.

The whole experimental data generation has been done for both homogeneous and heterogeneous phantoms.

The trained NN is interfaced with an output visualization module. The output is in terms of (Location, Size) pair and virtual image (of breast and tumor) visualization.

- If both values are positive in (Location, Size) pair (i.e., $(+ve, +ve)$) indicates tumor existence and corresponding virtual image showing the tumor position and size within breast dimension.
- If either or both values are negative in (Location, Size) pair (i.e., $(-ve, +ve)$ or $(+ve, -ve)$ or $(-ve, -ve)$) indicates healthy breast and corresponding virtual image of breast dimension only.

3. RESULTS

3.1. Homogenous Breast Phantom

The average absolute error is calculated using Equation (1).

$$E = \frac{1}{n} \sum t_n - y_n \tag{1}$$

where t_n is the target vector, y_n is the predicted value by the NN and n is the number of samples. However, the relative performance rate can be calculated using Equation (2).

$$E_i = \frac{\max(y_i, t_i) - \min(y_i, t_i)}{\max(y_i, t_i)} \tag{2}$$

where y_i are the predicted values and t_i are the targets.

The achieved experimental tumor existence detection rate is approximately 100%.

Using Equation (1), the absolute tumor size and location detection rates are 95.8% and 94.3% respectively, which is in agreement with the simulation results in [8]. Table 4 shows relative performance detection rate of tumor size using Equation (2). Negative value for actual tumor size means there is no tumor. Corresponding to the negative input (actual), the negative output value (predicted tumor size) insures the

Table 4. Relative performance detection accuracy of tumor size in the homogeneous breast phantom. Negative value means no tumor exists.

Data groups	Actual tumor size (mm)	Predicted tumor size (mm)	Relative performance %
Training data (partial)	6.00	6.31	95.09
	2.00	1.96	98.00
	−1.00	−0.95	100.00
	4.50	4.91	91.65
	1.00	1.91	52.36
	2.00	2.27	88.11
	4.50	4.92	91.46
	1.00	1.93	51.81
	6.00	6.31	95.09
	6.00	6.38	94.04
	−1.00	−0.95	100.00
	2.00	2.41	82.99
	6.00	6.36	94.34
Validating data	2.00	1.93	96.50
	2.00	1.99	99.50
	4.50	4.31	95.78
	6.00	6.11	98.20
	7.50	6.54	87.20
Testing data	6.00	6.53	91.88
	−1.00	−0.92	100.00
	2.00	1.92	96.00
	2.00	2.25	88.89
	7.50	6.54	87.20
	2.00	2.83	70.67

accuracy and efficiency of tumor detection rate in our system. This is true for all cases. The relative performance detection rate for tumor location is similar.

3.2. Heterogeneous Breast Phantom

The tumor existence detection rate of approximately 100% is also achieved in heterogeneous breast phantom experimental setup. Using Equation (1), the absolute tumor size and location detection rates are 93.4% and 93.1% respectively. It should be mentioned here that the most important achievement is the tumor existence detection in its possible earliest stage. The accuracy in detecting the exact location is not so important. Here inaccuracy by one or two centimeter is not severe as due to this further medical diagnoses or removal operation will not be affected much. The same principle applies to tumor size detection. As far as the tumor is detected, specifying the exact size is not crucial. Table 5 shows the relative performance accuracy of tumor location detection rate.

Figure 10 shows the GUI of our system output in terms of virtual image for heterogeneous breast phantom. It shows, a tumor of size 2 (mm) and location at 55 (mm along x-axis) is detected as: size 2.83 (mm) and location at 56.3 (mm) respectively.

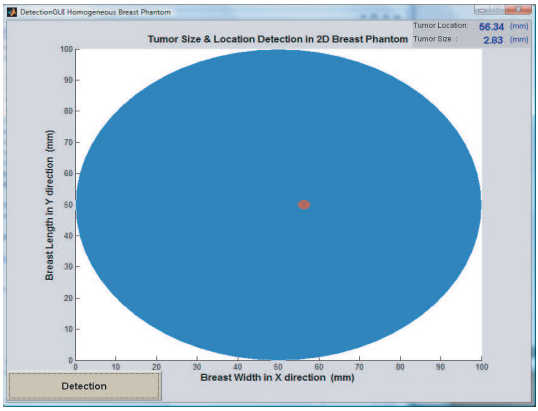

Figure 10. System output with GUI showing virtual image of a tumor of size 2.83 (mm) at location 56.3 (mm).

Figure 11 shows a comparison between the simulation [8] and experimental results for the homogenous breast phantom for various tumor sizes. Figure 12 shows similar results for various tumor locations. The simulation was conducted for homogeneous breast phantom only using planner waves to propagate through it. Both

figures show that the experimental results are sometimes better than or in agreement with the simulation results. Even though, the simulation setup is an ideal environment, the experiment work which is done in noisy normal room shows better results. This could be because of the use of actual UWB Tx-Rx, antennas, signals and DCT. Also, the number of signal value points obtained in the experimental work is

Table 5. Tumor location relative performance detection rate in the heterogeneous case.

Data groups	Actual tumor location (mm)	Predicted tumor location (mm)	Relative performance %
Training data (partial)	−1.00	−0.92	100
	20.0	20.5	97.56
	25.0	32.8	76.22
	55.0	54.3	98.73
	60.0	60.5	99.17
	10.0	18.9	52.91
	50.0	47.5	95.00
	30.0	30.4	98.68
	20.0	18.9	94.50
	75.0	70.5	94.00
	60.0	58.7	97.83
	25.0	21.8	87.20
	70.0	73.2	95.63
	−1.00	−0.92	100
	40.0	31.8	79.50
	10.0	19.8	50.51
	65.0	64.1	98.62
Validating data	20.0	20.9	95.69
	15.0	19.0	78.95
	60.0	59.2	98.67
	25.0	19.4	77.60
	60.0	66.5	90.23
Testing data	40.0	34.0	85.00
	−1.00	−0.92	100
	75.0	68.1	90.80
	15.0	21.0	71.43
	60.0	61.5	97.56
	55.0	21.2	38.55

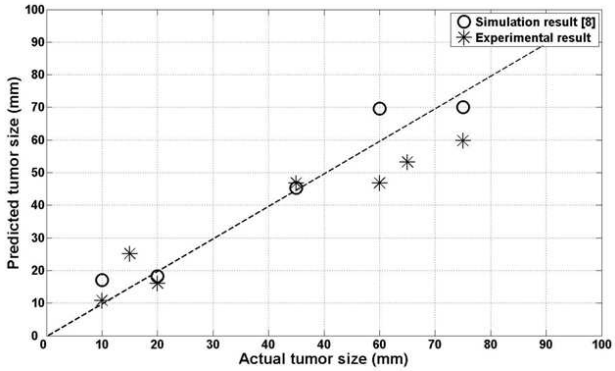

Figure 11. Some actual vs. predicted tumor sizes from both simulation and homogeneous experimental work.

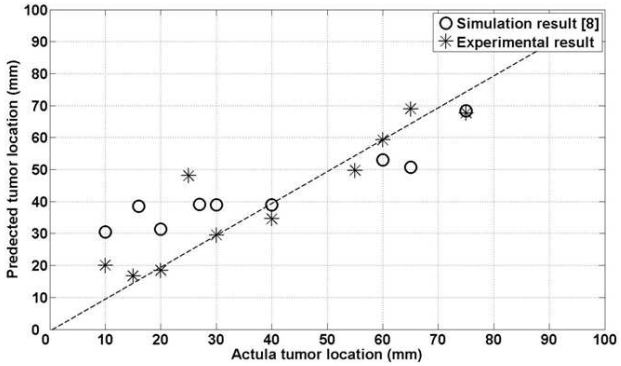

Figure 12. Some actual vs. predicted tumor locations from both simulation and homogenous experimental work.

much larger than the simulation work.

Comparison of our results with related experimental studies using homogeneous breast medium [1, 4] shows some improvement as shown in Table 6. Even though the experiments setup are not similar, our study shows 2.7% improvement in tumor size detection compared to results presented in [4], whereas it is about 0.3% improvement in tumor location detection. Result reported in [1] shows about 1.2% improvement in tumor location detection compared to our result. However, the tumor size detection is not included in that study. The previous studies have not investigated about the tumor existence detection performed instead they tested for location and/or size while tumor existence is already known. In our system, NN testing

Table 6. Comparison of tumor size and location detection rates (for homogeneous phantom) with other studies using Equation (1).

	Tumor size detection rate	Tumor location detection rate
Our study (homogeneous)	95.8%	94.3%
Study in [4]	93.1%	94%
Study in [1]	not reported	95.5%

set contains some signals correspond to tumor existence and some for tumor absence and approximately up to 100% tumor existence detection rate has been achieved.

4. CONCLUSION

This paper proposes a new, easy and cost-effective method to construct homogeneous and heterogeneous breast phantoms, and tumor using available materials. The tumor is constructed by controlling the water content ratio in the water-wheat flour mix. They are for temporary use as the water content migrates with time.

A VNA free complete system prototype is developed for experimental early breast tumor detection. It is user friendly, affordable and consists of UWB Tx-Rx with PC connectors, one PC and our developed software package module (installed in the PC) including interfacing, NN module and GUIs. So, the system is suitable to be used both by doctors in the hospital, and the end users at home for regular breast monitoring.

Experiments to detect tumors are performed in regular noisy room environment for both phantom cases using the developed system. The tumor existence, size and location detection rates for both cases are highly satisfactory with almost 100% assurance of early detection in case of any which has not been obtained in any previous work. Hence, the efficiency and superiority of our system is apparent followed by the very early detection and possible saving of precious human life in near future.

When detecting tumor existence, it is desirable to distinguish between the malignant and benign types. The same breast phantoms are currently under investigation to achieve this goal.

REFERENCES

1. Bindu, G., A. Lonappan, V. Thomas, C. K. Ananadan, and K. T. Mathew, "Active microwave imaging for breast cancer detection," *Progress In Electromagnetic Research*, Vol. 58, 149–169, 2006.
2. Lim, H. B., N. T. Nhung, E. Li, and N. D. Thang, "Confocal microwave imaging for breast cancer detection: Delay-multiply-and-sum image reconstruction algorithm," *IEEE Transaction on Biomedical Engineering*, Vol. 55, No. 6, 1697–1704, 2008.
3. Fear, E. C., X. Li, S. C. Hagness, and M. A. Stuchly, "Confocal microwave imaging for breast tumor detection: Localization of tumors in three dimensions," *IEEE Transactions on Biomedical Engineering*, Vol. 49, No. 8, 812–822, 2002.
4. Fear, E. C., J. Still, and M. A. Stuchly, "Experimental feasibility study of confocal microwave imaging for breast tumor detection," *IEEE Transactions on Microwave Theory and Techniques*, Vol. 51, No. 3, 887–897, March 2003.
5. Li, X., S. K. Davis, S. C. Hagness, D. W. Weide, and B. D. Veen, "Microwave imaging via space-time beam forming: Experimental investigation of tumor detection in multilayer breast phantoms," *IEEE Trans. Microwave Theory Techniques*, Vol. 52, No. 8, 1856–1865, 2004.
6. Xiao, X., "Study on the breast cancer detection by UWB microwave imaging," *Proceedings of the International Conference on Microwave and Millimeter Wave Technology, ICMMT2008*, Nanjing, China, April 21–24, 2008.
7. Sill, J. M. and E. C. Fear, "Tissue sensing adaptive radar for breast cancer detection-experimental investigation of simple tumor models," *IEEE Transactions on Microwave Theory and Techniques*, Vol. 53, No. 11, 3312–3319, 2005.
8. Alshehri, S. A. and S. Khatun, "UWB imaging for breast cancer detection using neural networks," *Progress In Electromagnetic Research C*, Vol. 7, 79–93, 2009.
9. O'Halloran, M., M. Glavin, and E. Jones, "Performance and robustness of a multistatic MIST beamforming algorithm for breast cancer detection," *Progress In Electromagnetic Research*, Vol. 105, 403–424, 2010.
10. O'Halloran, M., M. Glavin, and E. Jones, "Rotating antenna microwave imaging system for breast cancer detection," *Progress In Electromagnetic Research*, Vol. 107, 203–217, 2010.
11. Byrne, D., M. O'Halloran, E. Jones, and M. Glavin, "Transmitter-

grouping robust capon beamforming for breast cancer detection," *Progress In Electromagnetic Research*, Vol. 108, 401–416, 2010.

12. Lazaro, A., D. Girbau, and R. Villarino, "Wavelet-based breast tumor localization technique using a UWB radar," *Progress In Electromagnetic Research*, Vol. 98, 75–95, 2009.
13. Sha, L., E. R. Ward, and B. Story, "A review of dielectric properties of normal and malignant breast tissue," *Proceedings IEEE SoutheastCon*, 457–462, April 5–7, 2002.
14. Byrne, D., M. O'Halloran, M. Glavin, and E. Jones, "Data independent radar beamforming algorithms for breast cancer detection," *Progress In Electromagnetic Research*, Vol. 107, 331–348, 2010.
15. O'Halloran, M., M. Glavin, and E. Jones, "Channel-ranked beamformer for the early detection of breast cancer," *Progress In Electromagnetic Research*, Vol. 103, 153–168, 2010.
16. Klemm, M., I. Craddock, J. Leendertz, A. Preece, and R. Benjamin, "Radar-based breast cancer detection using a hemispherical antenna array — Experimental results," *IEEE Transactions on Antennas and Propagation*, Vol. 57, 1692–1704, 2009.
17. Lazaro, A., D. Girbau, and R. Villarino, "Simulated and experimental investigation of microwave imaging using UWB," *Progress In Electromagnetics Research*, Vol. 94, 263–280, 2009.
18. Lai, J. C., C. B. Soh, E. Gunawan, and K. S. Low, "Homogeneous and heterogeneous breast phantom for ultra-wideband microwave imaging applications," *Progress In Electromagnetic Research*, Vol. 100, 377–415, 2010.
19. Lazebnik, M., E. L. Madsen, G. R. Frank, and S. C. Hagness, "Tissue-mimicking phantom materials for narrowband and ultrawideband microwave application," *Physics in Medicine and Biology*, Vol. 50, 4258–4258, August 2005.
20. Time Domain Corporation, Comings Research Park, 330 Wynn Drive, Suite 300, Hantsville, Al 35805, USA.
21. Miyakawa, M., T. Ishida, and M. Wantanabe, "Imaging capability of an early stage breast tumor by CP-MCT," *Proceedings of the 26th Annual International Conference of the IEEE EMBS*, Vol. 1, 1427–1430, San Francisco, CA, USA, September 1–5, 2004.
22. Lazebnik, M., et al., "A large-scale study of the ultrawideband microwave dielectric properties of normal, benign and malignant breast tissues obtained from cancer surgeries," *Phys. Med. Biol.*, Vol. 52, 6093–6115, IOP Publishing, October 2007.

23. Bindu, G., A. Lonappan, V. Thomas, V. Hamsakkutty, D. K. Aanandan, and K. T. Mathew, "Microwave characterization of breast-phantom materials," *Microwave and Optical Technology Letters*, Vol. 43, No. 6, 506–508, December 2004.
24. O'Halloran, M., M. Glavin, and E. Jones, "Effects of fibroglandular tissue distribution on data-independent beamforming algorithms," *Progress In Electromagnetic Research*, Vol. 97, 141–158, 2009.
25. Lazebnik, M., et al., "A large-scale study of the ultrawideband microwave dielectric properties of normal breast tissues obtained from reduction surgeries," *Phys. Med. Biol.*, Vol. 52, 2637–2656, IOP Publishing, April 2007.
26. Dielectric Constants of Common Materials http: //www.flowmeterdirectory.com/dielectric_constant_01.html.
27. Conceicao, R. C., M. O'Halloran, E. Jones and M. Glavin, "Investigation of classifiers for early-stage breast cancer based on radar target signatures," *Progress In Electromagnetic Research*, Vol. 105, 295–311, 2010.
28. Conceicao, R. C., M. O'Halloran, M. Glavin, and E. Jones, "Comparison of planar and circular antenna configurations for breast cancer detection using microwave imaging," *Progress In Electromagnetic Research*, Vol. 99, 1–20, 2009.
29. Ahmed, N., T. Natarajan, and K. R. Rao, "Discrete cosine transform," *IEEE Transactions on Computers*, Vol. 32, 90–93, January 1974.